SIAM J. APPL. MATH.
Vol. 66, No. 3, pp. 921–944

STOCHASTIC MODELING AND SIMULATION OF TRAFFIC FLOW: ASYMMETRIC SINGLE EXCLUSION PROCESS WITH ARRHENIUS LOOK-AHEAD DYNAMICS*

ALEXANDROS SOPASAKIS† AND MARKOS A. KATSOULAKIS†

Abstract. A novel traffic flow model based on stochastic microscopic dynamics is introduced and analyzed. Vehicles advance based on the energy profile of their surrounding traffic implementing the "look-ahead" rule and following an underlying asymmetric exclusion process with Arrhenius spin-exchange dynamics. Monte Carlo simulations produce numerical solutions of the microscopic traffic model. Fluctuations play an important role in profiling observationally documented but, at the simulation level, elusive traffic phenomena. Furthermore, based on scaling and limit arguments we obtain a macroscopic description of this microscopic dynamics formulation which up to leading term of the expansions takes the form of integrodifferential Burgers or higher-order dispersive partial differential equations. We outline connections and comparisons of the hierarchical models presented here (microscopic, macroscopic) with other well-known traffic flow models.

Key words. traffic flow, look-ahead stochastic Arrhenius microscopic dynamics, Monte Carlo simulations

AMS subject classifications. 90B20, 60K30, 65C35, 65C05

DOI. 10.1137/040617790

1. Introduction and overview.

Building on the idea presented in [61], a new modeling approach of traffic flow is developed, which, based on Arrhenius microscopic stochastic dynamics [66], is adapted to vehicular traffic. We construct an asymmetric single exclusion process (ASEP) whose dynamics include interactions with other vehicles ahead ("look-ahead" rule). The model has remarkable attributes and similarities when compared to known observed traffic behavior and is able to predict most of the widely accepted traffic states at the microscopic level.

Traffic states that are commonly observed by researchers at the microscopic level are quite complex and at times even chaotic [22, 28, 29]. Some of the major traffic states that are commonly observed at the microscopic level are free flow, congested flow, synchronized traffic, and wide moving jams. Free flow is easily recognized by the ability of drivers to attain their desired speeds under very little, if any, interaction with other vehicles. Congested flow, in contrast, is characterized by heavy vehicular interactions and usually very low flows. In general in the regime above some critical density ($\approx$20% jam density), we usually observe the most interesting microscopic vehicular traffic phenomena. Among them, the phenomenon of synchronized traffic, as recently observed [29], may occur when above critical density and displays complex behavior. Synchronized traffic usually occurs at on ramps when vehicles are added to an already crowded highway. Although the corresponding flows are widely scattered, synchronized traffic is characterized by high vehicle flows and at the same time increasing vehicle densities [22, 27]. It has been observed [23, 28] that synchronized traffic breaks down (known as the "break-down" phenomenon) with a variety of "stop-

*Received by the editors October 27, 2004; accepted for publication (in revised form) June 28, 2005; published electronically March 3, 2006.
http://www.siam.org/journals/siap/66-3/61779.html
†Department of Mathematics and Statistics, Lederle Graduate Research Tower, University of Massachusetts, Amherst, MA 01003-9305 (sopas@math.umass.edu, markos@math.umass.edu). The research of the second author was partially supported by NSF-DMS-0413864 and NSF-ITR-0219211.

and-go" traffic waves and occurrence of even more chaotic phenomena [22, 28, 15]. Meta-stability and hysteresis [65, 9] effects (as vehicle densities increase) may also be associated with this behavior. Last, the so-called wide moving jams are localized structures moving upstream and are characterized by long (widthwise) waves whose "fronts are shorter than their width" [58]. Naturally vehicle speeds change sharply through the two fronts making up the wide moving jam. As those waves travel slowly upstream vehicles are forced to interact with a number of them. Wide moving jams appear also at densities above critical density [27, 29]. In general vehicles first transition from free flow to synchronized flow and then later, at a different location, we observe the transition to a wide moving jam [27, 58].

Attempts to model vehicular traffic date as far back as 1932 [19]. At first such attempts were mainly empirical and emphasized fitting parameters to the particular conditions at hand. However it is generally agreed that the "parameters of the model should be intuitively easy to calibrate and the corresponding values should be realistic" [22]. As a result, modeling approaches evolved and a variety of models and new approaches emerged, ranging from car-following to gas-dynamic to hydrodynamic and more recently cellular automaton to counter this problem.

Car-following (or follow-the-leader) models [17, 16, 54, 12, 69] appeared as a way of obtaining equations which can be used in a wider context than their (empirical) predecessors. As the name denotes, car-following models describe traffic behavior based on the vehicle leading closely up front. In some of these models [67] vehicles try to converge to their preferred (following) distance, relative to the vehicle in the front, thus creating an oscillatory behavior due to imperfect perception [29]. Clearly these models are not suitable, or designed, for large traffic streams.

The emergence of gas-dynamics-like (mesoscopic) [31, 25, 23, 64, 60, 59] and hydrodynamic-like (macroscopic) [52, 68] traffic models starting in the 1960s produced partial differential equations which attempt to describe traffic parameters of interest such as the density, velocity, and flow at larger time and spatial scales, thus encompassing larger traffic streams. Among them the fundamental model of Lighthill and Whitham [42], reflecting conservation of vehicles, is prominent. In its diffusive version [68], assuming a linear type of equilibrium velocity-density relationship [19], $V_{equil} = V_{max}(1 - c/c_{max})$ it takes the form of the Burgers equation,

$$\frac{\partial g}{\partial t} + g\frac{\partial g}{\partial r} = D\frac{\partial^2 g}{\partial r^2}, \tag{1.1}$$

where $D > 0$ is a diffusion constant, $g = V_{max}\,(1 - 2c/c_{max})$, and c denotes the density. We refer to [24] for further comments and references.

Optimal velocity models [47, 2, 64] emerged at almost the same time as car-following models. Newell [54] was the first to propose the following formulation for the equation of motion:

$$\frac{dx_j(t+\tau)}{dt} = V(\Delta x_j(t)),$$

where $x_j(t)$ is the position of vehicle j at time t and τ is a delay time. Here $\Delta x_j(t)$ is the headway of vehicle j at time t while V denotes a known optimal velocity rule. It has been shown [48] that some such optimal velocity traffic models can also be interpreted through the well-known mass transfer problem. Optimal velocity models have been used [47, 48, 34] to derive some of the well-known nonlinear wave equations such as Burgers, KdV, and modified KdV. Solutions of those nonlinear

wave equations are subsequently shown [48, 47] to describe different traffic regions: free flow, metastable region, unstable region. For an extended review of optimal velocity models see further comments and references in [48] and [6].

More recently, with the help of faster computers, cellular automaton (CA) microscopic traffic models have produced promising results when compared to traffic observations of similar spatial and time scales. Von Neumann introduced CA in 1950 in his abstract theory to study the logical conditions for self-reproducing machines [7]. It was, however, first due to Conway's game of life and later Wolfram [62, 70], which made CA well known in the dynamical systems community. The now famous rule CA 184, which has been studied in detail as a surface growth [36] (see also [14] for more comments), is widely implemented in CA traffic models. Since then the concept of CA has been applied and extended to model a wide variety of systems [39, 45].

To our knowledge [6] the first CA model for vehicular traffic was introduced by Cremer and Ludwig [8]. However, it was due to the contributions of Nagel and Schreckenberg [50] that CA models became widely known in traffic modeling. A number of improvements [32, 33, 49, 3] have been proposed since the original Nagel–Schreckenberg CA model, which also introduced random effects. These effects are deemed to better predict chaotic behavior of observed traffic at the microscopic scale. More recently a new CA, coded CA 184a, has been proposed by Nelson for traffic flow [53]. Similarly, development of discrete models proposed by Li [44], allows essential features of traffic to be captured and a better description of complex nonlinear phenomena to be studied.

In this work we extend the usual lattice-gas dynamics to vehicles. Based on an underlying stochastic model we reproduce some of the observed behavior of vehicular traffic when scrutinized under similar temporal and spatial scales. We assume a one-dimensional periodic (single-lane loop highway) lattice while we refer to [11] for generalizations (two-lane highway with entrances and exits). We start by obtaining suitable interpretations of many of the usual parameters of Ising systems and in many instances absorb as many of those parameters as possible to adapt our model to vehicular traffic observations. Special attention must be exercised to the application of the proper microscopic stochastic dynamics. Spin-exchange (diffusion) dynamics are therefore implemented to enforce conservation of vehicles. Overall we introduce the ASEP [13, 35, 40], guaranteeing that vehicles do not occupy the same site. An added novelty of this model is that vehicles are forced to move toward one direction since the dynamics, depending on spatial forward Arrhenius interactions, implement one-sided potentials and a look-ahead feature which can be considered to represent driver behavior. A variety of ASEP models without look-ahead Arrhenius interactions have been studied in [18]. Numerically we implement a kinetic Monte Carlo algorithm simulating aperiodic, consecutive (not parallel) microscopic stochastic dynamics. Among its many features the proposed stochastic model is able to predict spontaneous jam formation, "slow to start" (retarded acceleration) [63], and timely braking [58].

We also obtain kinetic mesoscopic PDEs derived in suitable asymptotic limits from the microscopic model which predict traffic observables for the appropriate validity ranges of these equations. Up to leading order we obtain Burgers and/or dispersive-type PDEs. We outline several connections between the hierarchical macroscopic models obtained through our expansions and other well-known traffic flow models [68, 54, 47, 34, 48, 28] and equations [26] of similar form. We examine these features in detail.

We start with an overview and derivation of the full model and present the details of the dynamics comprising our stochastic process in section 2. We subsequently

calibrate the free parameters of the stochastic model and produce the fundamental diagram (an important traffic engineering flow-density relationship) and other relevant solutions for our model in the numerical Monte Carlo simulations in section 3. In section 4 we obtain deterministic limit closures of our stochastic microscopic model, thus obtaining mesoscopic and macroscopic PDEs and systems of finite difference equations. Numerical comparisons of those models are presented in the same section. Final remarks and conclusions can be found in section 5. In the appendix we analyze briefly actual and theoretical data-gathering techniques which are in general of fundamental importance for the comparisons carried out in this work and elsewhere.

2. ASEP with Arrhenius look-ahead dynamics. We propose here an ASEP specifically equipped with conservative Arrhenius dynamics including a novel look-ahead parameter L. As a result we obtain a microscopic traffic flow model and its corresponding semigroup generator while introducing the notation to be used and general underlying assumptions.

We start by defining our physical space on a one-dimensional, periodic lattice, representing a one-lane loop highway. We partition our lattice into N cells, $\mathcal{L} = \{1, 2, \ldots, N\}$. On each of the lattice points $x \in \mathcal{L}$ we define an order parameter $\sigma(x)$ via

$$\sigma(x) = \begin{cases} 1 & \text{if a vehicle occupies site } x, \\ 0 & \text{if site at } x \text{ is empty (no vehicle).} \end{cases} \tag{2.1}$$

A spin configuration σ is an element of the configuration space $\Sigma = \{0,1\}^{\mathcal{L}}$ and we write $\sigma = \{\sigma(x) : x \in \mathcal{L}\}$ denoting by $\sigma(x)$ the spin at x.

Similarly to the Arrhenius dynamics for Ising systems [66] we let the interaction potential (which here will dictate the local behavior of vehicles) have the form

$$U(x, \sigma) = \sum_{\substack{y \in \mathcal{L} \\ y > x}} J(y - x)\sigma(y), \tag{2.2}$$

where J denotes an anisotropic short range intervehicle interaction potential,

$$J(x, y) = \gamma V\left(\gamma(y - x)\right), \quad x, y \in \mathcal{L}, \tag{2.3}$$

where $\gamma = 1/(2L+1)$ is a parameter prescribing the range of microscopic interactions and therefore L denotes the potential radius. Note that (2.2) in effect implements the interactions with vehicles up to range L ahead of the vehicle at position x, thus enforcing the look-ahead rule. Physically since a vehicle (or cell) length is taken to be 22 feet, then the look-ahead rule which is enforced by (2.2) allows drivers to see traffic at a physical distance which is $L \cdot 22$ feet ahead of their vehicle. Specifically we let $V : R \to R$ and set

$$V(r) = 0, \quad r \in R^{-} \quad \text{and} \quad V(r) = 0 \quad \text{for} \quad r \geq 1.$$

Note that the interaction potential $U(x)$ could be further enriched with the addition of an external potential h. This potential $h \equiv h(x,t)$ could vary in space but also time if so desired to account for temporal and spatial traffic situations (i.e., rush hour traffic).

There are several different choices for dynamics which we can employ: Arrhenius, Metropolis, Kawasaki, etc. We implement spin-exchange Arrhenius dynamics. Under this engine the simulation is driven based on the energy barrier a particle has

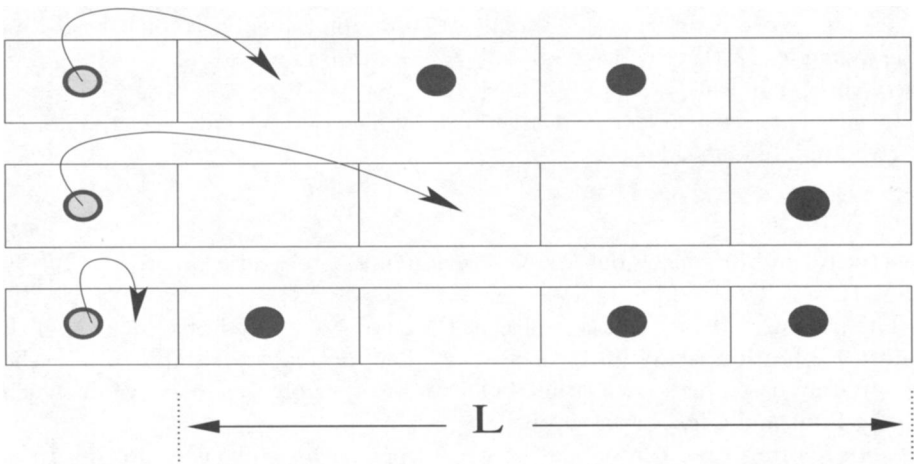

FIG. 1. *Simple schematic of the look-ahead rule (for $L = 4$ cells) pertaining to vehicle motion in the lattice for three different traffic examples. The process automatically simulates effects such as braking, acceleration, and simple exclusion rule through the interaction potential $U(x, \sigma)$ (2.2) for the provided range, L.*

to overcome in changing from one state to another. This energy barrier is found by calculating the potential energy of each vehicle based on (3.1) and performing a move only if that energy is higher than a given threshold. (Note that these dynamics are different from the usual Metropolis dynamics, where a move is encouraged whenever the energy difference between the current position and the new position is high enough.)

During such a spin-exchange between nearest neighbor sites x and y the system will actually allow the order parameter $\sigma(x)$ at location x to exchange value with the one at y. This is interpreted as advancing a vehicle from the site at x to the empty site at y. Note that based on the construction of our potential U it is not possible to move from an occupied site to another occupied cite; see Figure 1. In general, the rate at which a process will do this for spin-exchange Arrhenius dynamics is

$$c(x, y, \sigma) = \begin{cases} c_0 \exp[-U(x, \sigma)] & \text{if } y = x + 1, \text{ and } \sigma(x) = 1, \ \sigma(y) = 0, \\ & \text{if } \sigma(x) = 0 \ \ \sigma(y) = 1, \\ 0 & \text{otherwise} \end{cases} \tag{2.4}$$

The parameters comprising the dynamics here are

$$c_0 = 1/\tau_0 \tag{2.5}$$

with τ_0 the characteristic or relaxation time for the process and $U(x, \sigma)$ as in (2.2).

Overall given (2.4) and the dynamics just described the probability of spin-exchange between x and y during time $[t, t + \Delta t]$ is

$$c(x, y, \sigma)\Delta t + O(\Delta t^2). \tag{2.6}$$

Clearly for one-lane traffic y corresponds to either $x - 1$ or $x + 1$ in (2.4). Note that the exchange, due to the specific construction of the interaction potential J in (2.3), can take effect if and only if the location at x is occupied while the location at y is not. A simple schematic of the lattice and some simple interactions are provided in Figure 1. At the same time, vehicles are restricted (exclusion rule) with performing

an exchange move backward—an unrealistic move for vehicular traffic—by definition of the dynamics (2.4). Note we do not allow backward moves at all since they are not part of the dynamics.

In summary this model is determined by the characteristic time, interaction strength, and look-ahead

$$\tau_0, J_0 \text{ and } L,$$

respectively, and driven by our Arrhenius dynamics stochastic process $\{\sigma_t\}_{t\geq 0}$ with rate (2.4).

The parameter c_0 will allow us to set the maximum speed of vehicles (which we do in the calibration section (3.1)) while the other parameters L and J_0 will be chosen appropriately based on known traffic behavior or other physical constraints which we present in our numerical investigations.

More rigorously we can define the generator for this stochastic process $\{\sigma_t\}_{t\geq 0}$. Let f be an arbitrary test function defined on $L^\infty(\Sigma)$, where Σ is the configuration space $\Sigma = \{0,1\}^{\mathcal{L}}$. Then the generator, M, of the process is defined,

$$Mf(\sigma) = \sum_{x\in\mathcal{L}} c_0\sigma(x)(1-\sigma(x+1))\exp(-U(x,\sigma))[f(\sigma^{x,x+1}) - f(\sigma)] \tag{2.7}$$

with c_0 from (2.5) and

$$\sigma^{x,x+1} = \begin{cases} \sigma(y), & y \neq x, x+1, \\ \sigma(x+1), & y = x, \\ \sigma(x), & y = x+1, \end{cases}$$

denotes an exchange of the spins between locations x and $x+1$. We refer to [40, 41] for background on generators and exclusion processes.

3. Monte Carlo simulations and benchmarks. We now present numerical implementations of the microscopic stochastic traffic flow model derived in section 2. We start by physically interpreting the nondimensional model variables and subsequently calibrating our model for the free parameters τ_0, J_0 and L with respect to well-known quantities from real traffic data. Last, as a basic benchmark, we also obtain the fundamental diagram corresponding to the flow-density relationship dictated by our model.

In the simulations we choose a simple constant potential of the form

$$V(r) = \begin{cases} J_0 & \text{if } 0 < r < 1 \\ 0 & \text{otherwise} \end{cases} \quad \text{for} \quad J_0 > 0, \tag{3.1}$$

where J_0 is a parameter which based on its sign describes attractive repulsive or no-interactions. In our simulations we implement $J_0 > 0$, which implies that vehicles are attracted by the empty space in front of them. Note that (3.1) imposes only forward interactions and the dynamics (2.4) do not allow for backward moves. Thus vehicles move toward the empty space in the highway with an exclusion rule since we allow only one vehicle per site; see Figure 1. We have therefore created an ASEP [35] with interactions in one direction. In fact, the proposed dynamics reduce to an ASEP-type evolution if a particle/vehicle does not have any other vehicles in front of it beyond the interaction radius L in (2.3). In our numerical simulations we implement piecewise constant ($J_0 = 1$), short-range local interactions. However, we can also impose a V, in the form of a one-sided Maxwellian, which could be more realistic.

We let the actual physical length of each cell to be 22 feet. This allows for the average vehicle length plus safe distance. Therefore for a vehicle which has an average speed of 65 miles per hour we obtain a natural estimate of time to cross a cell,

$$\Delta t_{cell} = \frac{22 \text{ feet}}{65 \text{ miles/hour}} \approx \frac{1}{4} \text{ sec.} \tag{3.2}$$

In this work we start by modeling an infinite length road (ring road) with no entrances or exits so as to observe certain known traffic behavior and compare with other similar works [50].

Given the (one-sided) structure of the potential (2.2) we allow vehicles (or drivers) to be able to perceive traffic forward of their position up to a possible distance (look-ahead) of four cells or up to 88 feet—vehicle lengths plus safe distance. This is automatically implemented in the calculation of the interaction potential (2.2) and therefore plays a decisive role in the decision for making a move to a new location ahead through (2.4) and subsequently (2.6). However, we have also run simulations (not presented here) with a look-ahead of three and two vehicle lengths for comparison purposes. Further remarks regarding the influence of the look-ahead parameter can be found in section 4.4 and especially Figure 9.

We implement a kinetic Monte Carlo (KMC) simulation based on [4]. We refer to [61] for details on how the spin-exchange Arrhenius dynamics algorithm is applied. As expected, a KMC algorithm produces no null steps and therefore every iteration is a success. In that respect our KMC algorithm continues to choose and move vehicles at every step by skipping the idle waiting which occurs in usual Monte Carlo simulations and simply adjusting the simulation time by the appropriate amount, as if it had waited for that long. This is quite useful for the cases of high densities of vehicles or even more generally when a process reaches equilibration.

3.1. Calibration and validity. We start by calibrating our code through the free parameters J_0 and τ_0 by simulating a free-flow regime where we expect all vehicles to drive at their desired speed. We set such a speed to be 65 miles per hour. This is accomplished by the characteristic time τ_0, which allows us to calibrate the maximum velocity at which vehicles would like to drive assuming no other vehicles up front. Naturally, due to the stochasticity inherent in our simulation some vehicles will drive faster while some slower than the set limit of 65 miles per hour. As pointed out earlier the free parameter J_0 indirectly influences how drivers react to conditions in front of them and subsequently allows us to set the velocity of an upstream front (which researchers estimate it to be approximately -10 miles per hour [22, 58]). In Figure 2 we record all the parameters used and the average velocities of a stream of traffic which is initially randomly distributed under free-flow conditions. Note that for the chosen parameters $\tau_0 = .23$ and $J_0 = 6$ we obtain the desired velocity of 65 miles per hour and velocity out of a jam of ≈ -10 miles per hour. Also note that other pairs of τ_0 and J_0 are possible which easily adjust the traffic model for different standards set in other countries or regions.

3.2. Monte Carlo simulations. Using the calibrated parameters for J_0 and τ_0 from section 3.1 we now obtain the fundamental diagram (see the Appendix for details), the density—flow relationship in Figure 3, and the flow-velocity relationship in Figure 4. In general we can implement a number of different types of initial conditions which we make specific for each example considered. For these figures we use a random initial vehicle distribution and observe the behavior of the traffic stream as density increases incrementally.

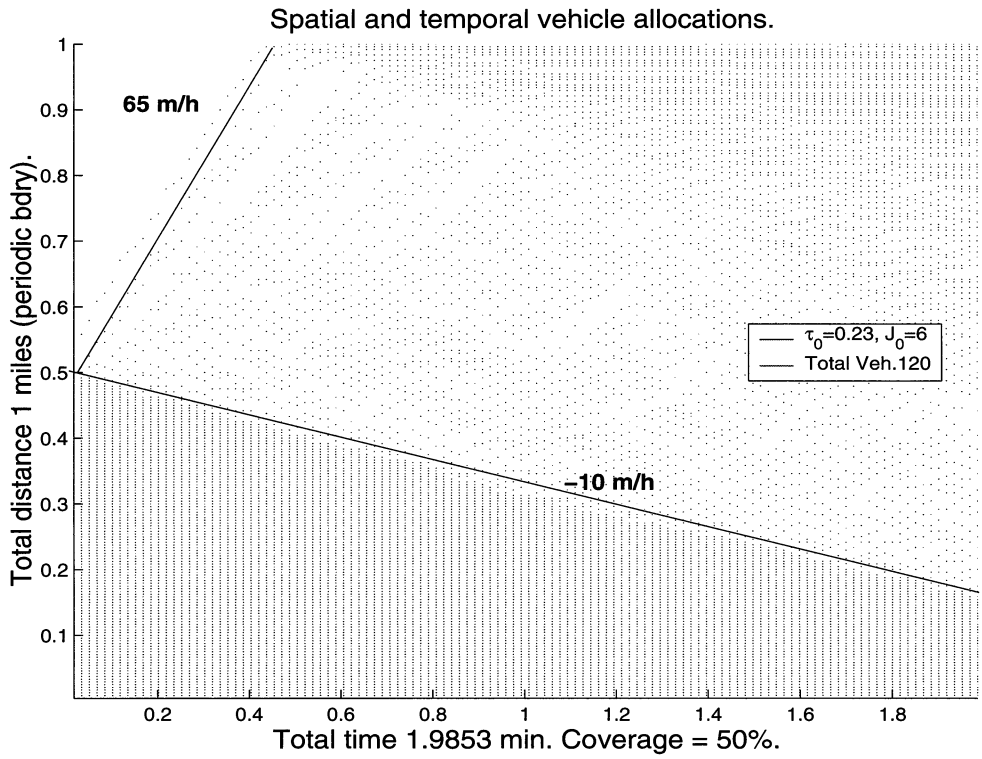

FIG. 2. *Calibration of parameters permitting a desired vehicle speed of* 65 *miles per hour and upstream front velocity of* ≈ -10 *miles per hour. We take a look-ahead of* $L = 4$. *Initial density corresponds to a traffic release problem (i.e., bumper-to-bumper vehicles up to* 0.5 *miles and no vehicles after that).*

It is of particular interest to analyze the simulated results for the well-established behavior of actual traffic at high densities, which includes stop-and-go waves, congested traffic, and other such interesting phenomena, all of which could be identified at the microscopic level. The phenomena observed at small time scales disappear in long averaged runs of the microscopic models. Cassidy [5] and Munoz and Daganzo [56] suggest how to eliminate two-regime flow by appropriately filtering the data. It is clear that these traffic states could not possibly be predicted, at their full complexity, as solutions of deterministic systems of differential equations [10] since they almost disappear as we aggregate observables. This is a very important point which should be emphasized. It is in fact possible that a given PDE traffic model could be just an extension (in the correct asymptotic limit) of a given microscopic model. In fact, we show how this can be done for our stochastic traffic flow model in the following section. Note, however, that caution is in order here since long-time averages may be unreliable due to the possible presence of phase transitions. In this model, since metastability is expected, for some concentration regimes (near c_{crit}), the simulations should be analyzed under small-time averages (see the appendix). Metastability, phase transitions, and hysteresis effects in general are quite difficult to conclusively detect and as such we propose to further study them in a forthcoming publication.

Several very interesting observations can be made from Figures 3 and 4. We compare our results with those of Nagel and Schreckenberg [50] but also with observations

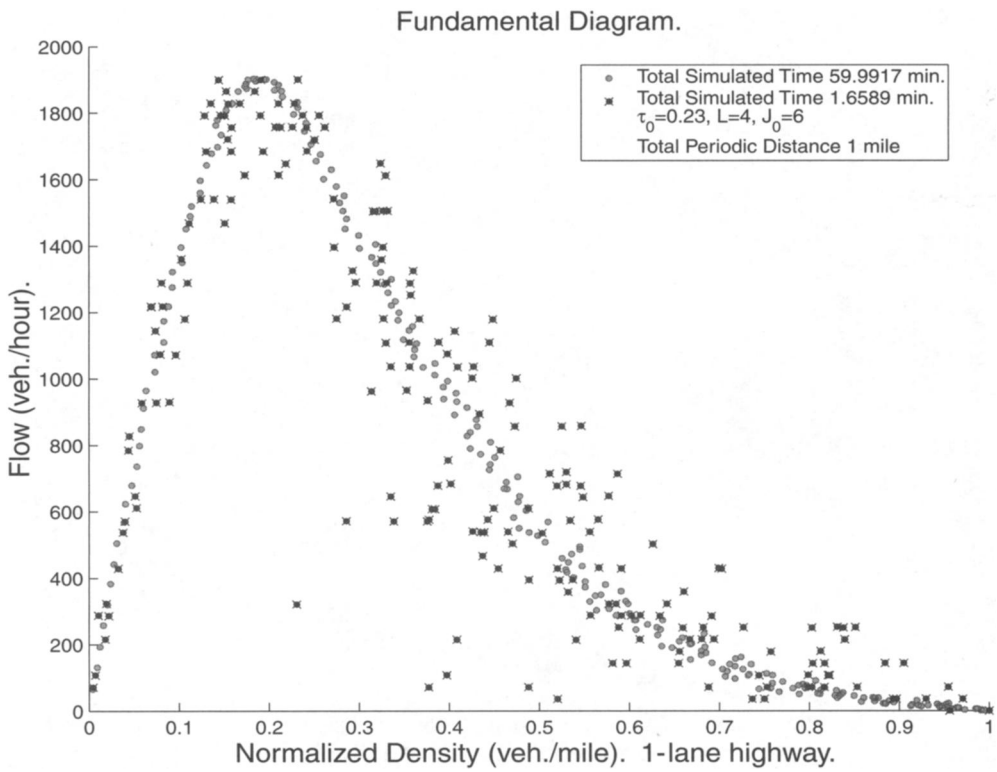

FIG. 3. *The flow density relationship for one-lane highway. Spatial periodic length of* 1 *mile, relaxation time* $\tau_0 = .23$*, interaction strength* $J_0 = 6$*, and look-ahead* $L = 4$ *cells. We superimpose two plots in this figure. In the first plot each point of the fundamental diagram is averaged over the usual* 1.65 *minutes aggregation time of data while in the second we display the long averaged flow and density for an aggregation time of a total of* 1 *hour. The aggregation time of* 1.65 *minutes was selected so that we can compare with observed data in* [51].

from Wiedemann [69] and observe qualitative agreement. Specifically, the region of free flow is clearly displayed up to approximately 50 vehicles per mile. Note here that the value of $c_{crit} = 50$ vehicles per mile is not forced on our simulation but instead is naturally created by the process dynamics through the calibration of the two parameters J_0 and τ_0. Similarly we observe a maximum vehicle flow of approximately 2000 vehicles per hour, which also agrees with observations [69], [51], and Figure 1(b) from [22]. (The aggregation time of 1.65 minutes was selected so that we can compare with observed data in [51].) An interesting question is whether this long averaged flux coincides with the equivalent mesoscopic partial differential equation of the stochastic limit. We answer this in section 4. The fluctuations in vehicle flows shown in Figures 3 and 4 are sizable for densities above c_{crit} and display a smeta-stable stop-and-go region. We should point out here that we did not fit parameters to obtain c_{crit} or q_{max} yet these parameters scale (for one-lane traffic) in agreement with observations of $c_{crit} \approx 50$ vehicles per miles and $q_{max} \approx 2000$ vehicles per hour [69].

In Figure 5 we display a close-up of vehicle trajectories for a congested traffic setup (50% jam density). In that figure we also observe that jams randomly form and sometimes disappear in time. In fact it can be easily calculated that these jams move backward in traffic with a speed of ≈ -10 miles per hour, which closely agrees with the reported speed of -15 ± 5 km per hour from [29, 58, 22].

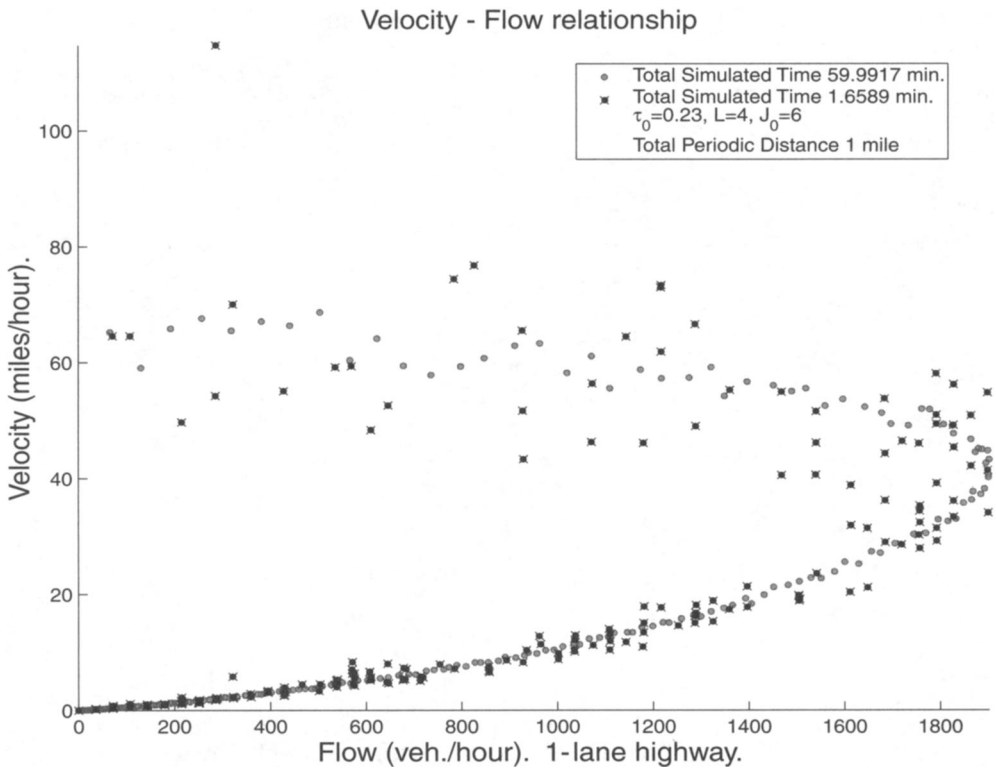

FIG. 4. *Velocity versus flow relationship for one-lane highway. Spatial periodic length of* 1 *mile, relaxation time* $\tau_0 = .23$*, interaction strength* $J_0 = 6$*, and look-ahead* $L = 4$ *cells. Once again we superimpose the* 1.65*-minutes aggregation time over the* 1*-hour aggregation time. This figure also compares favorably with observed data in* [51].

A consequence of the model versatility and ease of calibration presented is that calculations can be performed in real time for prediction purposes. The size of the traffic stream simulated in the numerical simulations here is small (< 3000 vehicles) and therefore the algorithm presented can easily produce real-time predictions. However, an improvement applicable for large traffic streams (> 3000 vehicles) is under development in [11], which uses a coarse graining idea and also produces real-time predictions. This has obvious important consequences since, as an example, we could possibly obtain the traffic input at a section of a highway in real time and immediately predict whether a traffic jam for the given highway capacity is imminent downstream, thus diverting traffic before the problem occurs.

4. Average behavior and deterministic closures. Although the emphasis of this paper is on new stochastic models we would like to establish connections with known CA and PDE models in various asymptotic regimes where mean field theory applies. Therefore we formally derive here a kinetic formulation of the stochastic model which is subsequently used to obtain an approximating finite difference (FD) scheme from (4.2) in the case of weak long-range interactions. Further, we also derive a PDE by a rescaling argument.

From our definition of a generator (2.7) we have

$$\frac{d}{dt}Ef(\sigma) = EMf(\sigma) \tag{4.1}$$

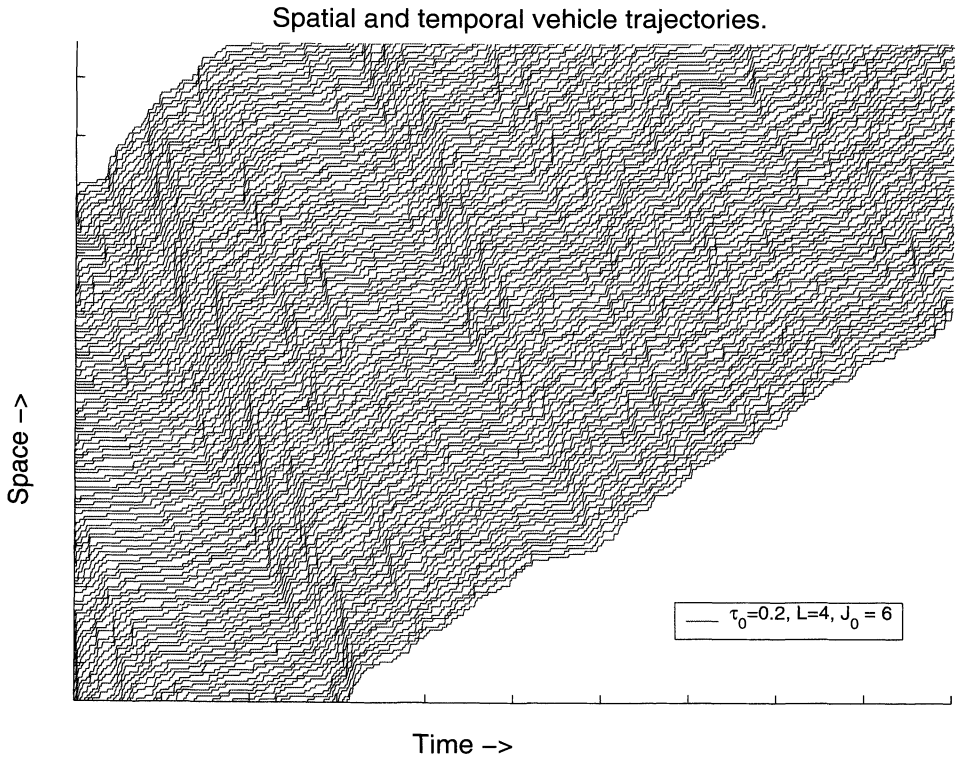

FIG. 5. *Vehicle stream lines in time and space. Spatial periodic length of* 1 *mile (corresponding to a total of* 240 *cells). We allow* 50% *initial capacity, relaxation time* $\tau_0 = .23$, *interaction strength* $J_0 = 6$, *and look-ahead* $L = 4$ *cells. Note the traffic waves in the stream displaying fronts and rarefactions.*

for any test function f, where $\sigma = \{\sigma_t : t \geq 0\}$ is the process corresponding to (2.7) and E denotes expected value. In particular we pick $f(\sigma) = \sigma(z)$ for z fixed in $\mathcal{L}$. Therefore

$$f(\sigma^{x,x+1}) = \sigma^{x,x+1}(z) = \begin{cases} \sigma(z), & x \neq z, x \neq z-1, \\ \sigma(z+1), & x = z, \\ \sigma(z-1), & x = z-1, \end{cases}$$

and based on (2.7) we have

$$f(\sigma^{x,x+1}) - f(\sigma) = \begin{cases} 0, & z \neq x, x+1, \\ \sigma(z+1) - \sigma(z), & x = z, \\ \sigma(z-1) - \sigma(z), & x = z-1. \end{cases}$$

By (2.7) and (4.1) we have the relation

(4.2)
$$\frac{d}{dt} E\sigma_t(z) = -Ec_0\sigma(z)(1-\sigma(z+1))e^{-U(z,\sigma)} + Ec_0\sigma(z-1)(1-\sigma(z))e^{-U(z-1,\sigma)}.$$

Note that relation (4.2) is exact and can be used to evaluate the closures discussed below. However, it is not yet a closed equation for $E\sigma_t(x) = \text{Prob}(\sigma_t(x) = 1)$.

4.1. Finite difference scheme. Suppose now that J (for J_0 fixed) has fairly long and weak interaction. We may assume that the stochastic process in (2.7) is a perturbation of the simple exclusion process considered in [40]. This process has a Bernoulli product invariant measure; thus at local equilibrium the probability measure is expected to be approximately a product measure. As in [57] we assume "propagation of chaos" for the microscopic system, in which case the fluctuations of the spins $\{\sigma(x), x \in \mathcal{L}\}$ about their mean values are independent and the law of large numbers formally applies. Thus the fluctuations of $\sum_{y\neq x} J(y-x)\sigma(y)$ about their mean will be small such that in the long-range interaction limit we have

$$Ee^{-U(x,\sigma)} = Ee^{-\sum_{y\neq x} J(y-x)\sigma(y)} \overset{N,L\to\infty}{\approx} e^{-\sum_{y\neq x} J(y-x)E\sigma(y)} + o_N(1). \tag{4.3}$$

Using the product property in (4.3) we formally obtain that the right-hand side of (4.2) becomes

$$-E\sigma(z)E(1-\sigma(z+1))c_0e^{-J\circ E\sigma(z)} + E\sigma(z-1)E(1-\sigma(z))c_0e^{-J\circ E\sigma(z-1)} + o_N(1), \tag{4.4}$$

where for an arbitrary function $v(z)$ we define

$$J\circ v(z) := \sum_{\substack{y\in\mathcal{L}\\ y>z}} J(y-z)v(y).$$

Next we drop $o_N(1)$ in (4.4) and define the density $u(z,t) = E\sigma_t(z)$. ($u(z,t)$ is the probability that site z is occupied at time t.) Then (4.2) and (4.4) give the following approximate semidiscrete FD scheme:

$$\begin{aligned}\frac{d}{dt}u(z,t) = &- c_0u(z,t)(1-u(z+1,t))\exp(-J\circ u(z,t))\\ &+ c_0u(z-1,t)(1-u(z,t))\exp(-J\circ u(z-1,t)) \quad \text{for all } z\in\mathcal{L}.\end{aligned} \tag{4.5}$$

Note that our semidiscrete FD scheme (4.5) is conservative. Simply define

$$F(z,t) = c_0u(z-1,t)(1-u(z,t))\exp(-J\circ u(z-1,t)) \tag{4.6}$$

and without loss of generality, assuming a periodic lattice of N nodes, we sum the right-hand side of (4.5) and obtain

$$\begin{aligned}\sum_{z=0}^{N-1} c_0[-F(z+1,t)+F(z,t)] &= c_0[F(0,t)-F(N-1,t)]\\ &= c_0[u(-1,t)(1-u(0,t))\exp(-J\circ u(-1,t))\\ &\quad -u(N-1,t)(1-u(N,t))\exp(-J\circ u(N-1,t))] = 0\end{aligned}$$

since $u(-1,t) = u(N-1,t)$ and $u(0,t) = u(N,t)$ due to spatial periodicity.

Note that based on (4.6) we can rewrite (4.5) as

$$\frac{du(z,t)}{dt} + F(z+1,t) - F(z,t) = 0.$$

4.2. PDE limit. We now formally obtain the resulting PDE from (4.5) and make connections with other known traffic flow models. We start by expanding the spatial variables in Taylor series. We set $h = \Delta x$ and use

$$u(z \pm 1, t) = u(z,t) \pm h u_z(z,t) + \frac{h^2}{2} u_{zz}(z,t) + \cdots .$$

Substituting into (4.5) we obtain

$$\frac{d}{dt}u + h\,[u(1-u)c_0 \exp(-J \circ u)]_z = O(h^2). \tag{4.7}$$

Rescaling time in (4.5),

$$t \to t h^{-1},$$

to absorb h and by omitting the $O(h^2)$ terms we have

$$\frac{d}{dt}u + [u(1-u)c_0 \exp(-J \circ u)]_z = 0 \tag{4.8}$$

$$\text{for } z \in R \quad \text{and} \quad J \circ u(z) = \int_z^\infty J(y-z)u(y)\,dy.$$

The transport equation obtained is

$$u_t + F(u)_z = 0, \tag{4.9}$$

where

$$F(u) = u(1-u)c_0 \exp(-J \circ u). \tag{4.10}$$

It is interesting to point out here that (4.10) under the simplest case of no interactions ($J_0 = 0$) corresponds to the well-known [68, 42] Lighthill–Whitham flux (1.1), thus producing a traffic stream formulation equivalent in form to the Burgers equation.

Note that in fact (4.5), when fully discretized, provides a natural finite difference scheme for (4.9),

$$\begin{aligned} u(z, t^{n+1}) = u(z,t^n) + \frac{\Delta t}{h}[&u(z-1,t^n)(1-u(z,t^n))c_0 \exp(-J \circ u(z-1,t^n)) \\ &- u(z,t^n)(1-u(z+1,t^n))c_0 \exp(-J \circ u(z,t^n))]. \end{aligned} \tag{4.11}$$

4.3. Stochastic versus semidiscrete approximation. We numerically compare the solutions of the stochastic model (4.2) against the semidiscrete scheme (4.5). In that respect we implement the same initial normalized density of vehicles (a traffic light release type) for both schemes with the following form:

$$u(z,0) = \begin{cases} 1 & \text{for cells in } 20 < z < 40, \\ 0 & \text{otherwise.} \end{cases} \tag{4.12}$$

The comparisons are performed under the assumption in (4.3) (i.e., $L = 240$ cells) for the semidiscrete scheme while the stochastic is averaged over several realizations to obtain an approximation of $E(\sigma_t(z))$. The solutions are shown in Figures 6 and 7 for the semidiscrete and stochastic models, respectively. The final profiles of these

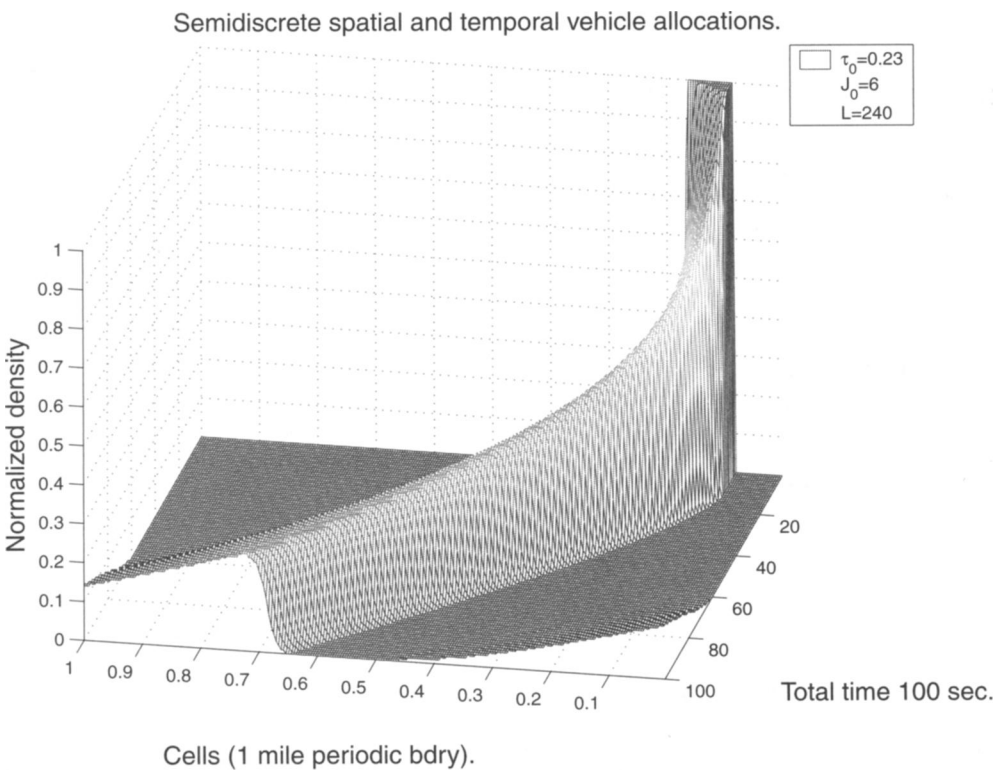

FIG. 6. *Solution of the semidiscrete scheme* (4.5) *in time and space for a traffic light type of initial condition* (4.12). *We set* $L = 240$ *based on the assumption in* (4.3). *Parameters:* $\tau_0 = .23$ *and* $J_0 = 6$.

solutions are compared in Figure 7. We clearly observe the expected rarefaction wave on one side and shock wave on the other.

In Table 4.1 we display the l_1 relative error estimates of the solutions of each model for different sizes of the interaction potential L at a specific time. The relative l_1 error is calculated from the final (in time) solutions of the semidiscrete and stochastic densities u_{sd} and u_{stoch}, respectively,

$$\frac{|u_{sd} - u_{stoch}|_{l_1}}{|u_{stoch}|_{l_1}} = \frac{\sum_z |u_{sd}(z, t_{final}) - u_{stoch}(z, t_{final})|}{\sum_z |u_{stoch}(z, t_{final})|}.$$

We observe the smallest relative errors in Table 4.1 for the case of $L = 240$. This is expected based on assumption (4.3). We compare the resulting stochastic microscopic (4.1) and FD PDE (4.11) models against each other and give possible connections with other well-known models in the following section.

4.4. Connections and comparisons between models and parameters. The task in this section is twofold. First we display possible connections between our derived models (4.1) and (4.11) with other well-known traffic flow models. Second, to further understand how parameters influence the fundamental diagram (more precisely the flux) of our derived mesoscopic formulations we also compare these formulations (4.10, 6.1) against each other to understand their possible limitations and range of predictions.

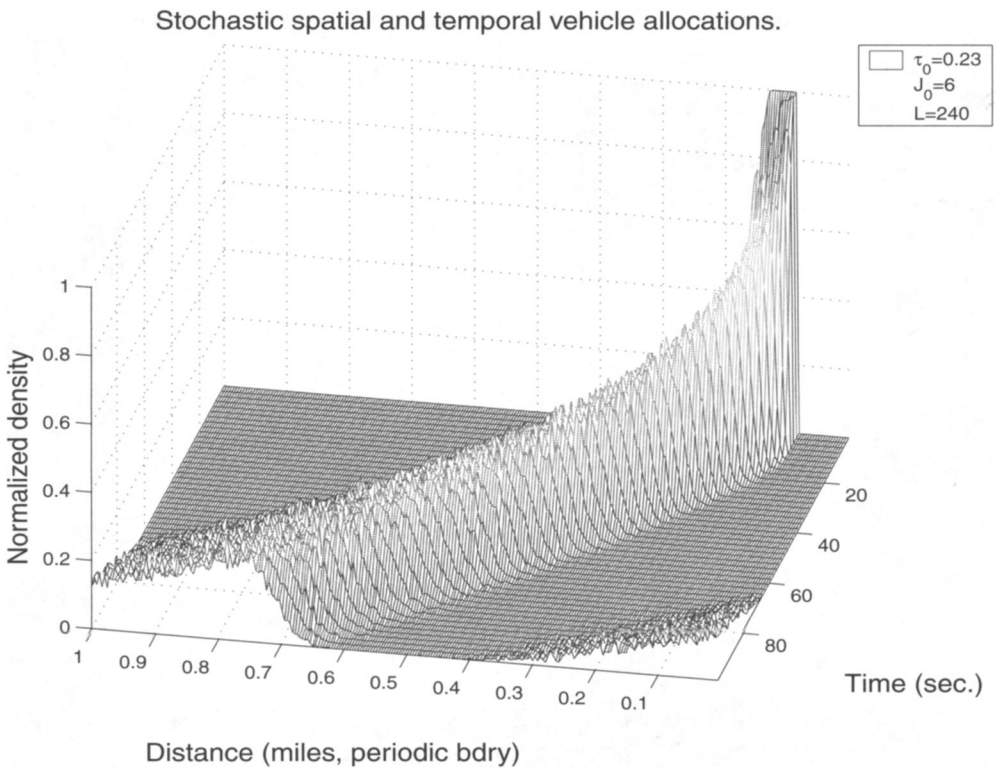

FIG. 7. *Solution of the stochastic model* (4.2) *in time and space for a traffic light type of initial condition* (4.12). *We average* 500 *realizations to produce the averaged density presented. Parameters:* $\tau_0 = .23, J_0 = 6$, *and* $L = 240$.

TABLE 4.1

Relative error of final solutions, similar to that presented in Figure 8, *comparing the semi-discrete FD scheme* (4.5) *against the stochastic model* (4.2) *solution for different sizes of the potential radius* L. *The stochastic solution has been averaged over* 500 *realizations. Other parameters:* $\tau_0 = .23$ *and* $J_0 = 6$.

Potential Radius L	240	100	50	10	4	1
l_1 Rel. Error	.0013	.0029	.0051	.0066	.0126	.02

4.4.1. Theoretical connections. We obtain here hierarchical connections with other well-known traffic flow models based on expansions of our underlying macroscopic equation (4.9) with (4.10),

$$u_t + [u(1-u)c_0 \exp(-J \circ u)]_z = 0. \tag{4.13}$$

We start by expanding the convolution term $J \circ u$,

$$J \circ u = \int_z^\infty V(y-z)u(y)\,dy \overset{x=y-z}{=} \int_0^\infty V(x)u(x+z)\,dx = J_0 u + J_1 u_z + J_2 u_{zz} + \cdots, \tag{4.14}$$

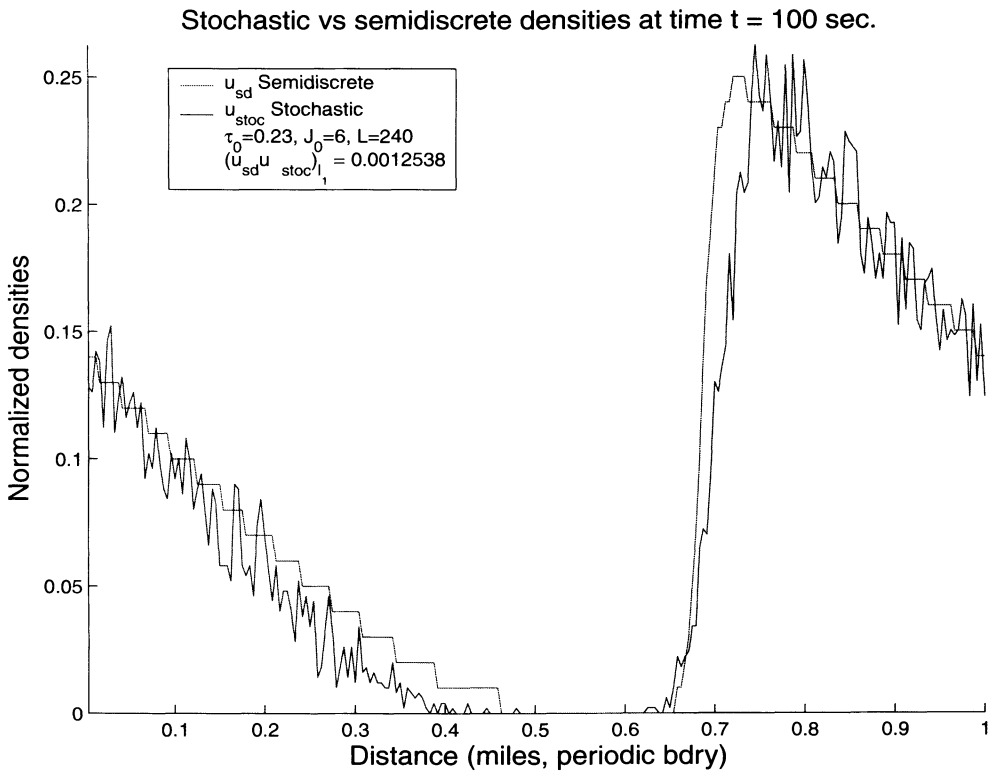

FIG. 8. *Density comparisons at final time $t = 100$ seconds. The error at that time in l_1 is also displayed. Once again, the stochastic is averaged over 500 realizations. Note the agreement between the solutions in both quantity and form. Parameters: $\tau_0 = .23$ and $J_0 = 6$ for $L = 240$.*

where assuming $V > 0$ (recall that the positive uniform potential we use here (3.1) implies that vehicles are attracted to the empty space in front of them) gives

(4.15)
$$J_0 = \int_0^\infty V(x)\,dx > 0, \quad J_1 = \int_0^\infty xV(x)\,dx > 0 \quad J_2 = \int_0^\infty \frac{x^2}{2}V(x)\,dx > 0.$$

We can therefore approximate the exponential as

$$e^{-J\circ u} \approx e^{-[J_0u+J_1u_z+J_2u_{zz}]} = e^{-J_0u}e^{-J_1u_z-J_2u_{zz}} \approx e^{-J_0u}[1 - J_1u_z - J_2u_{zz}],$$

which based on (4.13) gives the higher-order traffic flow model

$$(4.16)\quad u_t + c_0[u(1-u)e^{-J_0u}]_z = c_0[J_1u(1-u)e^{-J_0u}u_z]_z + c_0[J_2u(1-u)e^{-J_0u}u_{zz}]_z$$

with J_0, J_1, and J_2 from (4.15). Note that (4.16) is a third-order dispersive PDE with diffusion which is similar in form to the PDEs derived from optimal velocity models and usually referred to as modified KdV in [47, 48, 54].

We make general remarks below about the behavior of (4.16) as well as the more general (4.13) under different scales and/or parameters:

- Assuming first that there are no interactions $J = 0$ in the potential (4.10) of (4.13) we obtain $F(u) = c_0u(1-u)$, which gives the well-known diffusive Lighthill–Whitham or Burgers equation flux.

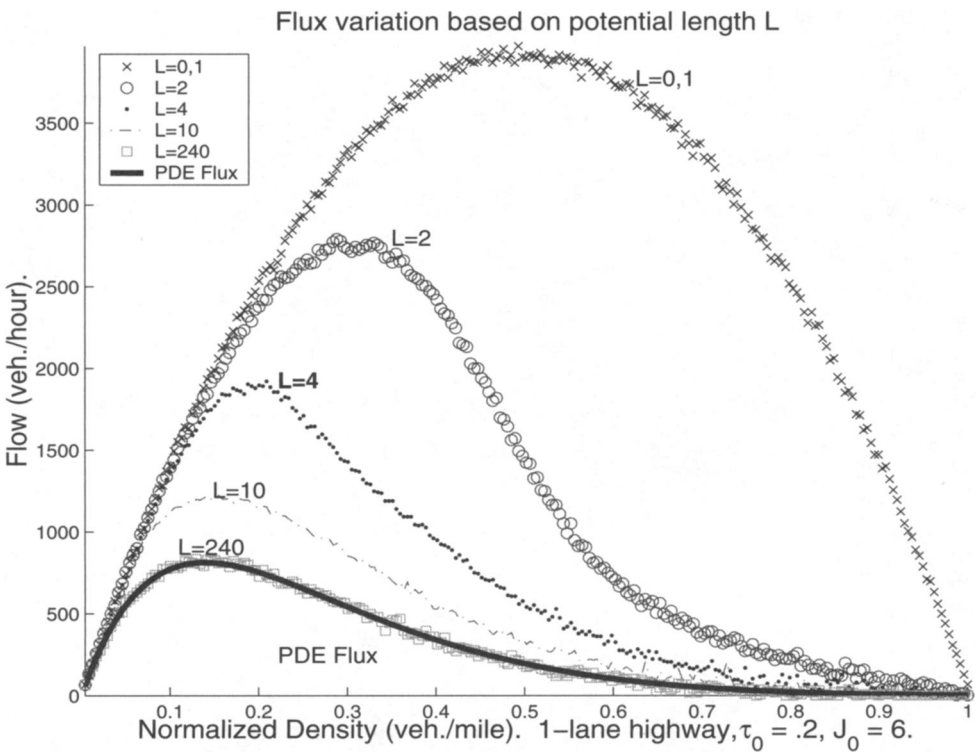

FIG. 9. *Long time averages. Comparing how the flux* (6.1) *changes with respect to increasing* L. *We set* $J_0 = 6, \tau_0 = .23$ *and run all microscopic simulations for the same total time and under the same initial conditions before plotting the flow per concentration. Note that for long-range interactions we observe that the PDE flux* (4.10) *coincides with the long-range interaction* ($L = 240$) *microscopic model flux* (4.17) *which fluctuates around it.*

- In the opposite case, however, of long-range interactions between vehicles, $L = N$, we obtain the following nonlocal flux from (4.10):

$$F(u) = c_0 u(1-u)\exp(-J_0\bar{u}). \tag{4.17}$$

  As we will see below (see Figure 9), under this long-range interaction case the flux of the stochastic model and that of the PDE (4.9, 4.10) agree.
- Note further that the hyperbolic equation obtained by including terms up to J_0 in the convolution (4.14) (disregarding J_1, etc.),

$$u_t + c_0[u(1-u)\exp(-J_0 u)]_z = 0, \tag{4.18}$$

  has a nonconvex flux. Indeed note in Figure 10 that if $J_0 \geq 3$ the flux is neither convex nor concave.
- If on the other hand we include terms up to order J_1 in (4.14), then (4.16) takes the form of a nonlinear diffusive Lighthill–Whitham type equation [68, 54, 48].
- Returning to the higher-order dispersive PDE (4.16) we note the similarities with other usual higher-order traffic flow models found in [34, 47, 48, 28, 38], although the coefficients obtained here include nonlinearities. Coherent structures can emerge as solutions of (4.16) which are similar to Figures 7 and 6 and

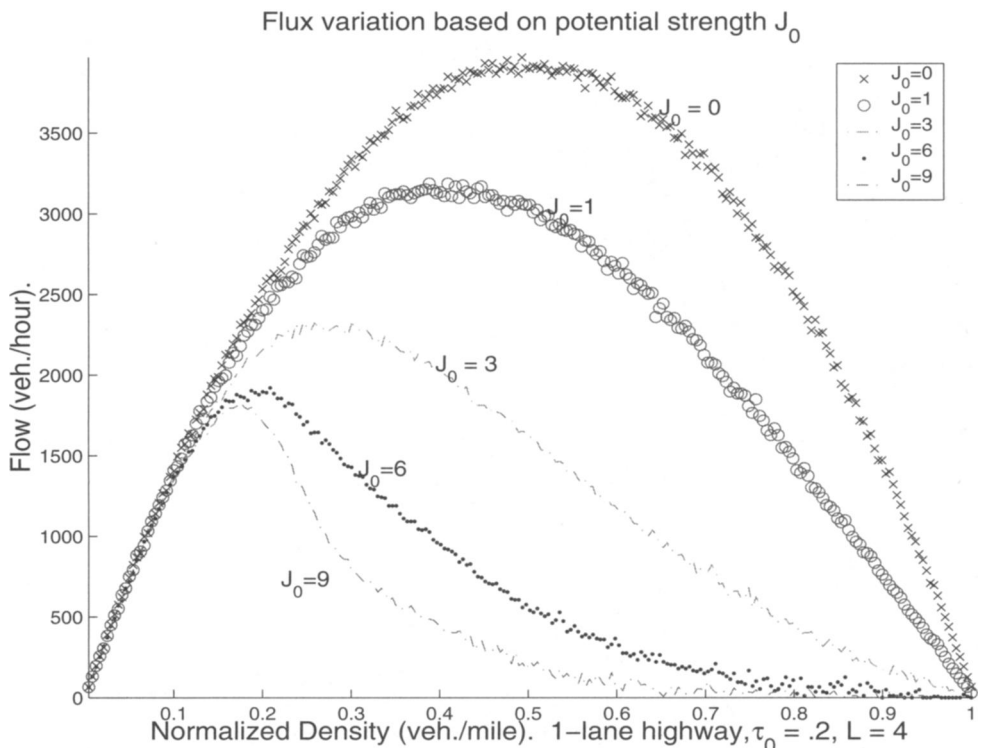

FIG. 10. *Long time averages. Comparing the influence of potential strength J_0 in the stochastic flux* (6.1). *In these comparisons we keep $L = 4$ and run all microscopic simulations for the same total time before plotting the flow per concentration.*

especially the profile density solution presented in Figure 8. It is known that traveling wave solutions of the Payne–Whitham model [37], [28] with nonconcave fundamental diagrams, which resemble the form of our higher-order PDEs, are asymptotically stable under small perturbations for a subcharacteristic type of condition [43]. It would be interesting to further examine traveling wave solutions of (4.13) as well as the higher-order approximation (4.16) and compare them with observed soliton, kink-antikink, or mixtures of other density solutions as have been noted in [34, 47, 28].

- Further, we remark that equations similar in form to (4.16) have also been studied in [26]. Diffusive and dispersive KdV type equations are emerging from Chapman-Enskog expansions of hyperbolic models with coexisting diffusion and relaxation contributions. The structure of the wave solutions which are shown to emerge for the dispersive, KdV type, equation presented there consists of enhanced solitary waves.

4.4.2. Numerical comparisons of fluxes. Clearly the microscopic model contains the maximum amount of information while the PDE is a rough averaging of the same system. It is also important, in terms of applicability of each model, to identify the range of parameters for which the PDE corresponds to our microscopic description. In that respect we expect certain parameters such as the interaction potential radius, the interaction size L, and the potential strength J_0 to be of significance. We

therefore display, in Figure 9, numerical simulations of the microscopic model predictions for different potential lengths L while keeping all other parameters the same. In that same figure we also plot the flux as obtained from our PDE formulation for a uniform potential strength value of $J_0 = 6$ and $\tau_0 = .23$ (to match the value implemented in our stochastic simulations). Note that, remarkably, the PDE flux and the microscopic flux corresponding to $L = 240$ (the maximum number of potential length) coincide (excluding the small fluctuations)! Respectively we also note that the PDE is a reasonable approximation for any microscopic model with $L > 10$ look-ahead. This is unfortunate, however, since physically we do not expect that drivers would (or even could) have a perception of traffic up front for more than possibly five vehicles. Notably the discrepancy between the microscopic and PDE fluxes is substantial for $L \approx 100$ cells or less. Such differences between long and short values for L have also been recorded in [66] for catalytic surface diffusion models.

We similarly examine how the potential strength J_0 influences the corresponding flux for either formulation (4.1) and (4.9) in Figure 10. We plot the microscopic flux for potential length of $L = 4$, which is more appropriate for actual traffic conditions. The case of $J_0 = 6$ connects Figure 9 to Figure 10 and allows for comparisons between the two. It is interesting to note how the expected concavity of traffic flow flux changes in Figure 10 as potential strength increases. In fact for values of $J_0 \geq 3$ the flux is neither concave not convex. Observe this loss of convexity also for $L \geq 2$ in Figure 9, thus producing a richer behavior than the typical Lighthill–Whitham (or Burgers) type traffic model predicts. On the other hand, in both Figures 9 and 10 we obtain one of the most basic traffic flow fluxes, the diffusive Lighthill–Whitham [68] (or Burgers) flux for the trivial case of either $J_0 = 0$ or $L = 0, 1$.

We also note the similarities of the simulated flux depicted in Figure 10 obtained here for $J_0 = 0$ and $J_0 = 6$ with Figures 2 and 3 from [50], respectively, as well as Figure 2 from [44]. Similar such agreement is also observed between Figure 10 (case of $J_0 = 6$) here and the observed data in Figure 1(b) and simulations in Figure 8 of [22].

5. Conclusions. In this work we have presented a stochastic microscopic model for traffic flow. The modeling and subsequent Monte Carlo simulations relied on simple calibration procedures of just three parameters: the potential interaction length of J_0, the relaxation time τ_0, and the look ahead L. Note that J_0 indirectly influences the desired speed of vehicles while τ_0 and L set the speed as vehicles are emerging out of a jam. Based on these settings we were able to produce realistic fundamental diagrams, for one-lane traffic, with qualitatively meaningful flows ($q_{max} \approx 2000$ vehicles per hour and $c_{crit} \approx 50$ vehicles per mile) which display many of the observed traffic states including phenomena such as stop-and-go traffic, spontaneous jam generation, retarded acceleration [63], and timely braking [58]. Overall the ease of calibration and richness of solution behavior make this stochastic model valuable in terms of describing, even at this simple one-lane setting, complex traffic flows.

Furthermore we derived (in the weak, long-range interactions limit) the corresponding macroscopic traffic model from our microscopic stochastic description. Subsequently we compared the solutions of each model for a variety of parameters making connections, for those regimes, with other well-known CA and PDE models for traffic flow. We obtain, up to leading order terms, hierarchical macroscopic diffusive and/or dispersive PDEs which resemble other well-known traffic flow models [68, 54, 28] of the same order. It would be interesting to examine our hierarchical macroscopic models (4.18), (4.16), and (4.13) for coherent structure solutions exhibiting behavior similar to that observed in [26, 48, 47, 28] (solitons, kink-antikink, etc.).

Last we point out that the simulations presented here can be performed in real time for the current one-lane traffic model proposed but also for multilane traffic which will be presented in a forthcoming work [11]. Extending the current one-dimensional stochastic microscopic model to multilane traffic will further allow us to directly compare our simulated results with available observational data [51, 69]. To further improve the model we also include entrances and exits by implementing two different, nonconservative (in contrast to the conservative spin exchange studied here) dynamics mechanisms: adsorption/desorption and surface diffusion.

6. Appendix: Data gathering and analysis techniques. The underlying method of recording, comparing, and analyzing traffic data for both the simulations and the observations is of paramount importance and must be clearly explained. Studies have been curried out by Athol [1] and more recently others [20, 46, 53] regarding proper data collecting procedures and underlying assumptions put forth in theory and in practice.

Observational traffic data can be obtained via a variety of methods: visual observations (video cameras), single or double loop detectors, magnetic overhead detectors, satellites, etc. In the majority, traffic data are gathered via detector loop techniques. In the case of double detector loops, for instance, pneumatic tubes (or, more recently, point detectors) are placed in close proximity on the highway and each is connected to a detector which records occurrences as vehicles pass on top of each tube. Quantities of interest that need to be determined from the collected data are usually the flow and velocity.

In general (regardless of detection method) the flow is measured as the number of vehicles $n(\tau)$ passing a detector at a given time interval τ via

$$q = \frac{1}{\tau} n(\tau) \tag{6.1}$$

(therefore flow cannot be found based on a single snapshot of vehicles over a length of interval). Usually flow is reported in number of vehicles per hour although the actual time length of recorded observation is much smaller (1/2 to 2 minutes). As a result some concerns have been raised regarding sustainability of such high volumes when data correspond to measurements over time intervals which are less than 15 minutes [21].

Average velocity on the other hand requires observations over both time and space. There are two ways to calculate velocity: time mean speed and space mean speed. As the name suggests, we calculate the time mean speed and space mean speed respectively through

$$\bar{u}_\tau = \frac{1}{N} \sum_{i=1}^{N} u_i \quad \text{and} \quad \bar{u}_s = \frac{s}{\frac{1}{N} \sum_{i=1}^{N} t_i}.$$

Here N denotes the number of time observations, s is the total distance covered in that time, and t_i is the corresponding time per observation. Note that in terms of (6.1) the following holds: $\tau = \sum_i t_i$. It is important to note here that the two definitions for mean speed provided above differ, as shown by Wardrop [67], by the ratio of the variance to the mean of the space mean speed,

$$\bar{u}_\tau = \bar{u}_s + \frac{\sigma_s^2}{\bar{u}_s}.$$

Therefore although they are similar for free-flow conditions they actually differ, especially near the highest flow regimes [20], for the key regions of stop-and-go and traffic breakdown. In practice double loop detectors are well suited to collect correctly space mean speeds. In this work (for comparative and other reasons which become clear below) we report our findings by computing space mean speed instead of time mean speed.

Density on the other hand is a quantity which is quite hard to measure empirically [46] and can be measured only along a length [20]. Having flow and space mean speeds, collected as described above, it is not uncommon to estimate the density from the well known macroscopic formula ("fundamental identity") as originally developed by Wardrop [67],

$$q = c\bar{v}. \tag{6.2}$$

A lot has been written regarding (6.2) but most importantly, as pointed out by Hall [20, p. 10], "its use has often exceeded the underlying assumptions." Clearly by applying (6.2) researchers introduce an assumption in terms of scales, ranges, and even continuity of observed variables [55] for which such an equation is valid. The validity of (6.2) is therefore sometimes questionable and its application varies among researchers, based on concentration, [30] (away from jam concentrations), [58]. The underlying problem of applying (6.2) to obtain the concentration is that (6.2) holds under "some very restrictive conditions" [20] which among other things imply that both space and time measurement intervals approach zero.

If point measurements are taken the best way [46] to estimate density is to instead calculate the lane occupancy, OC, of the traffic stream [20, 46]. Occupancy is the fraction of time that vehicles are over the detector,

$$OC = \frac{\text{total time detector is occupied by vehicle}}{\text{total study time}} = \frac{(L+D)/v}{\text{headway}} = c(L+D),$$

where L denotes the average vehicle length, D the detector length, and v the speed. (The headway is understood here as a time headway.) Therefore vehicle density c is found as

$$c = \frac{OC}{L+D}. \tag{6.3}$$

It is important to point out a common discrepancy: "almost all the theoretical work done prior to 1985 either ignores occupancy ... or else uses it ... as a surrogate for, density. On the other hand much of the freeway traffic management work ... (practical as opposed to theoretical work) relied on occupancy" [20].

In the simulations presented in our work we use virtual detectors in an effort of reproducing real traffic data collection procedures. As a result we place our virtual detector in a specific cell of our lattice and collect data on observables at that cell. Flow is computed based on (6.1) while density is found through calculation of occupancy as explained above and in the same fashion as done in [50] and similar other works. The data are averaged over small intervals of time (which we make precise in each of the presented simulations) as in real traffic data collection practices. In this work we simulate a closed round road without entrances or exits (race track) which we initialize with a specified total density (which naturally remains constant through the simulation) of randomly distributed vehicles. The fundamental diagrams are constructed by collecting data with a given density and then increasing that density and repeatedly restarting the complete simulation over again.

Acknowledgments. The first author would like to thank Chalmers Institute of Technology and Goteborg University, where part of this work was carried out during the summer of 2004. The first author would also like to thank Professor Paul Nelson for insightful discussions and comments during the preparation of this work.

REFERENCES

[1] P. Athol, *Interdependence of certain operational characteristics within a moving traffic stream*, Highway Research Record, 72 (1972), pp. 58–97.
[2] M. Bando, K. Hasebe, A. Hakayama, A. Shibata, and Y. Sugiyama, *Dynamical model of traffic congestion and numerical simulation*, Phys. Rev. E, 51 (1995), pp. 1035–1042.
[3] R. Barlovic, L. Santen, A. Schadschneider, and M. Schreckenberg, *Metastable states in cellular automata for traffic flow*, Eur. J. Phys. B, 5 (1998), pp. 793–800.
[4] A. B. Bortz, M. H. Kalos, and J. L. Lebowitz, *A new algorithm for Monte Carlo simulations of ising spin systems*, J. Comput. Phys., 17 (1975), pp. 10–18.
[5] M. J. Cassidy, *Bivariate relations in nearly stationary highway traffic*, Transportation Research B, 32 (1998), pp. 49–59.
[6] C. Chowdhury, L. Santen, and A. Schadschneider, *Statistical physics of vehicular traffic and some related systems*, Phys. Rep., 329 (2000), p. 199.
[7] E. F. Codd, *Cellular Automata*, Academic Press, New York, 1968.
[8] M. Cremer and J. Ludwig, *A fast simulation model for traffic flow on the basis of Boolean operation*, Math. Comput. Simulation, 28 (1986), p. 297.
[9] C. F. Daganzo, M. J. Cassidy, and R. L. Bertini, *Some traffic features at freeway bottlenecks*, Transportation Research B, 33 (1999), pp. 25–42.
[10] C. F. Daganzo, *Requiem for second-order fluid approximations of traffic flow*, Transportation Research B, 29 (1995), pp. 277–286.
[11] N. Dundon and A. Sopasakis, *Stochastic modeling and simulation of multi-lane traffic*, in progress.
[12] L. C. Edie, *Following and steady-state theory for non-congested traffic*, Oper. Res., 9 (1961), pp. 66–76.
[13] M. R. Evans, N. Rajewsky, and E. R. Speer, *Exact Solution of a Cellular Automaton for Traffic*, arXiv:cond-mat/9810306.
[14] H. Fukś, *Exact Results for Deterministic Cellular Automata Traffic Models*, arXiv: comp-gar/9902001.
[15] N. H. Gardner and N. H. Wilson, eds., *Freeway Speed Distribution and Acceleration Noise-Calculations from a Stochastic Continuum Theory and Comparison with Measurements*, Elsevier, New York, 1987.
[16] D. C. Gazis, R. Hermann, and R. W. Rothery, *Nonlinear follow-the-leader models of traffic flow*, Oper. Res., 9 (1961), pp. 545–567.
[17] D. L. Gerlough and M. J. Huber, *Traffic Flow Theory*, Technical Report 165, Transportation Research Board, Washington, DC, 1975.
[18] L. Gray and D. Griffeath, *The ergodic theory of traffic jams*, J. Statist. Phys., 105 (2001), pp. 413–452.
[19] B. N. Greenshields, *A study of traffic capacity*, in Proceedings of the 14th Annual Meeting of the Highway Research Board, 1934, pp. 448–474.
[20] F. L. Hall, *Traffic Flow Theory*, Chapter 2, Federal Highway Administration, Washington, DC, 1996, pp. 2–34.
[21] *Highway Capacity Manual*, Transportation Research Board, Washington, DC, 1985.
[22] D. Helbing, A. Hennecke, V. Shvetsov, and M. Treiber, *Micro- and macrosimulation of freeway traffic*, Math. Comput. Modelling, 35 (2002), pp. 517–547.
[23] D. Helbing and M. Treiber, *Gas-kinetic-based traffic model explaining observed hysteretic phase transition*, Phys. Rev. Lett., 81, 1998, pp. 3042–3045.
[24] D. Helbing, *Gas-kinetic derivation of Navier-Stokes-like traffic equations*, Phys. Rev. E, 53 (1995), pp. 2366–2381.
[25] R. Illner, A. Klar, and T. Materne, *Vlasov-Fokker-Planck models for multilane traffic flow*, Commun. Math. Sci., 1 (2003), pp. 1–12.
[26] S. Jin and J. G. Liu, *Relaxation and diffusion enhanced dispersive waves*, Proc. Roy. Soc. London A, 446 (1994), pp. 555–563.
[27] B. S. Kerner, S. L. Klenov, and D. E. Wolf, *Cellular automata approach to three-phase traffic theory*, J. Phys. A, 35 (2002), pp. 9971–10031.

[28] B. S. Kerner and P. Konhäuser, *Structure and parameters of clusters in traffic flow*, Phys. Rev. E, 50 (1994), pp. 54–83.
[29] B. S. Kerner and H. Rehborn, *Experimental properties of phase transitions in traffic flow*, Phys. Rev. Lett., 79 (1997), pp. 4030–4033.
[30] B. S. Kerner, *Dependence of Empirical Fundamental Diagram on Spatial-Temporal Traffic Patterns Features*, arXiv: cond-mat/0309018.
[31] A. Klar and R. Wegener, *Kinetic derivation of macroscopic anticipation models for vehicular traffic*, SIAM J. Appl. Math., 60 (2000), pp. 1749–1766.
[32] W. Knospe, L. Santen, A. Schadschneider, and M. Schreckenberg, *Towards a realistic microscopic description of highway traffic*, J. Phys. A., 33 (2000), pp. L477–L485.
[33] W. Knospe, L. Santen, A. Schadschneider, and M. Schreckenberg, *Single-vehicle data of highway traffic: Microscopic description of traffic phases*, Phys. Rev. E, 65 (2002), 056133.
[34] T. Komatsu and S. Sasa, *Kink soliton characterizing traffic congestion*, Phys. Rev. E, 52 (1995), pp. 5574–5582.
[35] J. Krug and P. A. Ferrari, *Phase transitions in driven diffusive systems with random rates*, J. Phys. A, 29 (1996), pp. L465–L471.
[36] J. Krug and H. Spohn, *Universality classes for deterministic surface growth*, Phys. Rev. A, 38 (1988), pp. 4271–4283.
[37] R. D. Kühne, *Macroscopic freeway model for dense traffic-stop-start wave and incident detection*, in Ninth International Symposium on Transportation and Traffic Theory, 1984, pp. 21–42.
[38] D. A. Kurtze and D. S. Hong, *Traffic jams, granular flow, and soliton selection*, Phys. Rev. E, 52 (1995), pp. 218–221.
[39] M. Duff and K. Preston, *Modern Cellular Automata: Theory and Applications*, Plenum, New York, 1984.
[40] C. Landim and C. Kipnis, *Scaling Limits of Interacting Particle Systems*, Springer, Berlin, 1999.
[41] T. M. Liggett, *Interacting Particle Systems*, Springer, Berlin, 1985.
[42] M. J. Lighthill and G. B. Whitham, *On kinematic waves* ii: *A theory of traffic flow on long crowde roads*, Proc. Roy. Soc. London Ser. A, (1955), pp. 317–345.
[43] T. Li and H. Liu, *Stability of a traffic flow model with non-convex relaxation*, Commun. Math. Sci., 3 (2005), pp. 101–118.
[44] T. Li, *Nonlinear dynamics of traffic jams*, Phys. D., 207 (2005), pp. 41–51.
[45] J. Marro and R. Dickman, *Nonequilibrium Phase Transitions in Lattice Models*, Cambridge University Press, Cambridge, UK, 1999.
[46] W. R. McShane and R. P. Roess, *Traffic Engineering*, Prentice-Hall, Englewood Cliffs, NJ, 1990.
[47] M. Muramatsu and T. Nagatani, *Soliton and kink jams in traffic flow with open bondaries*, Phys. Rev. E, 60 (1999), pp. 180–187.
[48] T. Nagatani, *The physics of traffic jams*, Rep. Prog. Phys., 65 (2002), p. 1331–1386.
[49] K. Nagel and M. Paczuski, *Emergent traffic jams*, Phys. Rev. E, 51 (1995), pp. 2909–2918.
[50] K. Nagel and M. Schreckenberg, *A cellular automaton model for freeway traffic*, J. Phys. I, 2 (1992), pp. 2221–2229.
[51] K. Nagel, D. E. Wolf, P. Wagner, and P. Simon, *Two-lane traffic rules for cellular automata: A systematic approach*, Phys. Rev. E, 58 (1998), pp. 1425–1437.
[52] P. Nelson, *Synchronized traffic flow from a modified Lighthill–Whitham model*, Phys. Rev. E, 61 (2000), p. R6052–R6055.
[53] P. Nelson, *On two-regime flow, fundamental diagrams and kinematic-wave theory*, in progress.
[54] G. F. Newell, *Nonlinear effects in theory of car following*, Oper. Res., 9 (1961), pp. 209–229.
[55] G. F. Newell, *Applications of Queueing Theory*, Chapman and Hall, London, 1982.
[56] J. C. Muñoz and C. F. Daganzo, *Structure of the transition zone behind freeway queues*, Transportation Sci., 37 (2003), p. 312–329.
[57] O. Penrose, *A mean-field equation of motion for the dynamic ising model*, J. Statist. Phys., 63 (1991), pp. 975–986.
[58] A. Schadschneider, *Traffic flow: A statistical physics point of view*, Phys. A, 312 (2002), pp. 153–187.
[59] A. Sopasakis, *Unstable flow theory and modeling*, Math. Comput. Modell., 35 (2002), pp. 623–641.
[60] A. Sopasakis, *Formal asymptotic models of vehicular traffic model closures*, SIAM J. Appl. Math., 63 (2003), pp. 1561–1584.
[61] A. Sopasakis, *Stochastic noise approach to traffic flow modeling*, Phys. A, 342 (2004), pp. 741–754.

[62] D. STAUFFER, *Computer simulations of cellular automata*, J. Phys. A, 24 (1991), pp. 909–927.
[63] M. TAKAYASU AND H. TAKAYASU, *Phase transition and $1/f$ noise in one dimensional asymmetric particle dynamics*, Fractals, 1 (1993) pp. 860–866.
[64] M. TREIBER, A. HENNECKE, AND D. HELBING, *Derivation, properties and simulation of a gas-kinetic based non-local traffic model*, Phys. Rev. E, 59 (1999), pp. 239–253.
[65] J. TREITERER AND J. A. MYERS, *The hysteresis phenomenon in traffic flow*, in Proceedings of the 6th ISTT, Sydney, Australia, D. J. Buckley, ed., A. W. Reed, London, 1974, pp. 13–38.
[66] D. G. VLACHOS AND M. A. KATSOULAKIS, *Derivation and validation of mesoscopic theories for diffusion of interacting molecules*, Phys. Rev. Lett., 85 (2000), pp. 3898–3901.
[67] J. G. WARDROP, *Some theoretical aspects of road traffic research*, in Proceedings of the Institut. of Civil Engineers, Part II, 1952, pp. 325–378.
[68] G. B. WHITHAM, *Linear and Nonlinear Waves*, Wiley, New York, 1974.
[69] R. WIEDEMANN, *Simulation des straßenverkehrsflusses*, Schriftenreihe des Instituts für Verkenhrswesen der Universität Karlsruhe, Germany, 1974.
[70] S. WOLFRAM, *Cellular Automata and Complexity*, Addison-Wesley, Reading, MA, 1994.